ADVANCED FUNCTIONAL MATERIALS

www.afm-journal.de

Versatile Electronic Skins for Motion Detection of Joints Enabled by Aligned Few-Walled Carbon Nanotubes in Flexible Polymer Composites

Hongfei Zhu, Xuewen Wang, Jia Liang, Hongling Lv, Huayu Tong, Lianbo Ma, Yi Hu, Guoyin Zhu, Ting Zhang, Zuoxiu Tie, Zheng Liu, Qingwen Li, Liwei Chen, Jie Liu,* and Zhong Jin**

Here, novel multifunctional electronic skins (E-skins) based on aligned few-walled carbon nanotube (AFWCNT) polymer composites with a piezoresistive functioning mechanism different from the mostly investigated theory of "tunneling current channels" in randomly dispersed CNT polymer composites are demonstrated. The high performances of as-prepared E-skins originate from the anisotropic conductivity of AFWCNT array embedded in flexible composite and the distinct variation of "tube-to-tube" interfacial resistance responsive to bending or stretching. The polymer/AFWCNT-based flexion-sensitive E-skins exhibit high precision and linearity, together with low power consumption (<10 μW) and good stability (no degradation after 15 000 bending–unbending cycles). Moreover, polymer/AFWCNT composites can also be used for the construction of tensile-sensitive E-skins, which exhibit high sensitivity toward tensile force. The polymer/AFWCNT-based E-skins show remarkable performances when applied to monitor the motions and postures of body joints (such as fingers), a capability that can find wide applications in wearable human–machine communication interfaces, portable motion detectors, and bionic robots.

1. Introduction

Electrical sensors built on flexible substrates that can translate ambient information such as mechanical deformation,[1] temperature,[2] or humidity[3] into digital signals are termed as electronic skins (E-skins).[4–6] Potential applications in soft robotics,[7] wearable health-monitoring technologies,[8–10] and touch-on displays[11,12] have resulted in a dramatic increase in the research efforts to design and fabricate E-skins. There are several E-skins operation modes under hot investigation: piezoresistive,[13,14] capacitive,[5,15–17] piezoelectric,[18,19] and triboelectric.[20]

Piezoresistive E-skins consisting of composite elastomers have received a great amount of attention due to their inherent flexibility, precision, chemical stability, and their simple, scalable, and cost-effective fabrication processes.[14,21] Most research on this sensing mode has focused on pressure-sensitive[16,22] or tensile-sensitive[23,24] E-skins. The functioning basis of piezoresistive E-skins under external stress is primarily attributed to the variation of interfacial resistance and conductive channels between conductive fillers, such as carbon black,[25] metal nanoparticles,[26] carbon nanotubes (CNTs),[12,16,24,27,28] and so on. Randomly dispersed conductive fillers in insulating elastomers are possible to be driven by external mechanical force to become close with each other and form tunneling conductive channels.[14] Compared with pressure-sensitive E-skins, flexion-sensitive and tensile-sensitive E-skins that can detect the movement of joints are receiving less but rapidly increasing attention, because they will be crucial components for smart wearable devices[29] and soft robotics[26] in the future.

In this work, we demonstrate that the arrays of aligned few-walled CNTs (AFWCNTs, with diameter of 3–5 nm)[30] can serve

Dr. H. Zhu, Dr. J. Liang, Dr. H. Lv, H. Tong, L. Ma, Y. Hu, G. Zhu, Dr. Z. Tie, Prof. J. Liu, Prof. Z. Jin
Key Laboratory of Mesoscopic Chemistry of MOE and Collaborative Innovation Center of Chemistry for Life Sciences
School of Chemistry and Chemical Engineering
Nanjing University
Nanjing 210093, China
E-mail: j.liu@duke.edu; zhongjin@nju.edu.cn

Dr. X. Wang, Prof. Z. Liu
School of Materials Science and Engineering
Nanyang Technological University
50 Nanyang Avenue, 639798, Singapore

Dr. T. Zhang, Prof. Q. Li, Prof. L. Chen
Suzhou Institute of Nano-Tech and Nano-Bionics
Chinese Academy of Sciences
Suzhou 215123, China
E-mail: lwchen2008@sinano.ac.cn

Prof. J. Liu
Department of Chemistry
Duke University
Durham, NC 27708, USA

DOI: 10.1002/adfm.201606604

as efficient anisotropic conductive fillers better than randomly dispersed CNTs in flexible composites for the fabrication of high-performance E-skins. The as-prepared semitransparent flexion-sensitive E-skin possesses many advantages, including high fatigue durability, high precision, low power consumption (<10 μW), and simple fabrication process. In addition to flexion-sensitive E-skin, the polymer/AFWCNT composites can also be applied for constructing tensile-sensitive E-skins for the detection of stretching with large extension ratios.

2. Results and Discussions

Instead of single-walled or multiwalled CNTs, AFWCNT arrays were used in this work owing to their unique advantages: (1) The preparation and adhesion of uniform AFWCNT array on polymer substrate are much easier than multiwalled CNTs.[30,31] (2) Different from single-walled CNTs that may exhibit metallic or semiconductive properties, AFWCNT arrays only show metallic and Ohmic behavior. (3) The packing density of AFWCNT bundles is normally lower than single-walled CNT bundles, therefore the interfacial resistance of AFWCNT bundles can be more easily changed by bending. Many polymers are suitable to serve as the matrix for AFWCNT composites. In this work, polymethyl methacrylate (PMMA) was chosen as a demonstration, owing to its good film-forming properties, high transparency, and easy processing. Piezoresistive flexion-sensitive E-skins based on PMMA/AFWCNT composite were fabricated on polyethylene terephthalate (PET) substrate, as shown in **Figure 1**a and described in the Experimental Section. Figure 1b shows the optical images of an AFWCNT array drawn from a FWCNT forest[30,31] grown on a SiO_2/Si substrate (top) and the AFWCNT array transferred onto PET substrate (bottom). The transferred parallel AFWCNT array was further treated with alcohol vapor to reinforce the van der Waals interaction between AFWCNT film and PET substrate, as shown in the scanning electron microscopy (SEM) image of Figure 1c. The atomic force microscopy (AFM) peak-to-valley roughness of pristine AFWCNT array on PET substrate was about 200 nm (Figure 1d). Subsequently, a thin layer of PMMA (200 nm thick) was spin-coated onto AFWCNT array to obtain a PMMA/AFWCNT composite film with smooth surface. Through AFM characterization, it was observed that some AFWCNTs were exposed on the surface of composite film, as shown in Figure 1e. The exposed AFWCNTs can act as the conductive connections between metal electrodes, as confirmed by the conductive AFM mapping (Figure 1f) with an applied bias voltage of 3.0 V between the AFM tip and the composite film. Figure 1g shows an optical image of an as-prepared PMMA/AFWCNT E-skin on PET substrate with a pair of aluminum (Al) top-electrodes deposited by thermal evaporation. Notably, the fabrication process of PMMA/AFWCNT composite E-skin is simple and scalable.

The schematic 3D structure of as-prepared flexion-sensitive E-skin is illustrated in **Figure 2**a. The electrical properties of E-skin were characterized by monitoring its current

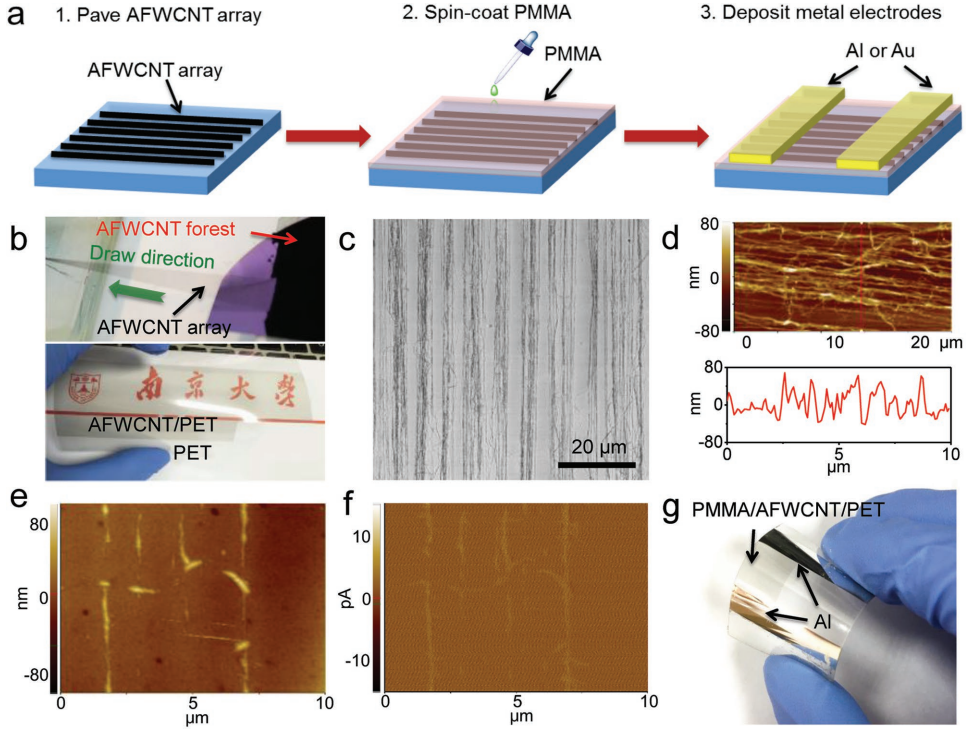

Figure 1. Fabrication process and morphology of flexion-sensitive E-skins based on PMMA/AFWCNT composite. a) Schematic illustration of the fabrication process. b) Optical images of an AFWCNT array drawn from a FWCNT forest (top) and a bended PET substrate with AFWCNT array attached on the surface (bottom). c) SEM image of AFWCNT array paved on PET after alcohol treatment. d) Topographic AFM image of the surface features of AFWCNT array paved on PET. e) Topographic AFM image of PMMA/AFWCNT composite and f) corresponding conductive AFM image at the bias voltage of 3.0 V. g) Optical image of a bended flexion-sensitive E-skin based on PMMA/AFWCNT composite.

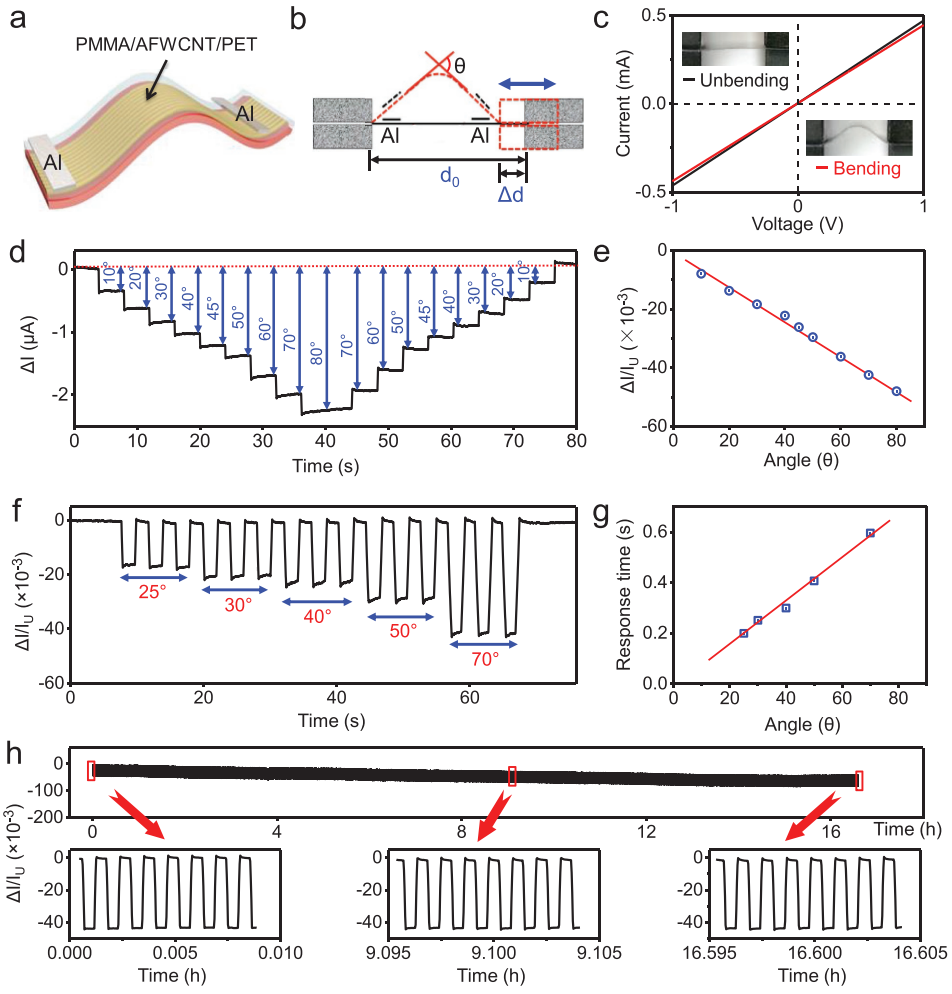

Figure 2. Performances of flexion-sensitive E-skins based on PMMA/AFWCNT composite. a) Illustration of the 3D structure of PMMA/AFWCNT composite-based flexion-sensitive E-skin. b) Schematic diagram of the E-skin in unbending (solid lines) and bending states (dashed lines and curves), respectively. c) *I*–*V* curves and optical images of the E-skin in unbending ($\theta = 0°$) and bending ($\theta = 70°$) states. d–g) Bending tests of the flexion-sensitive E-skin at a fixed applied voltage of 0.1 V. d) Current change ΔI of the E-skin as a function of time when the bending angle θ was changed stepwisely. e) Normalized current change $\Delta I/I_U$ of the E-skin calculated from panel (d) as a function of bending angle θ; the hollow circles represent actual experimental data and the red line represents linearly fitted data. f) $\Delta I/I_U$ as a function of time during three repeated bending–unbending cycles at various bending angles. g) Response time of flexion-sensitive E-skin from unbending state to different bending states measured in panel (f); the hollow rectangles represent actual response time and the red line represents linearly fitted data. h) Aging experiment of flexion-sensitive E-skin for 15 000 bending–unbending cycles with a bending angle of 70° (top figure); the three bottom figures show some typical cycles at the initial, middle, and ending stages of the testing process, respectively.

change under an applied voltage when bending the device by a motor-controlled stepper. The stepper propelled one end of the E-skin back and forth with the other end fixed for cycling between bending and unbending states (Figure 2b). The initial distance between the two clips of the stepper in unbending state was termed as d_0 and the moving distance of the stepper in bending state was Δd. The bending angle θ was defined as the external angle of the two ends of bended E-skin (Figure 2b). The conductive networks of AFWCNT bundles in PMMA/AFWCNT composite film show an Ohmic-conduction behavior between the metal electrodes, as presented by the *I*–*V* curves in unbending ($\theta = 0°$) and bending ($\theta = 70°$) states (Figure 2c; the magnified *I*–*V* curves in the range of 0–0.1 V are shown in Figure S2 in the Supporting Information). At the same applied voltage, the current of E-skin in bending state is lower than that in unbending state. The currents of E-skin in unbending and bending states are defined as I_U and I_B, respectively, and the real-time current change is termed as $\Delta I = I - I_U$, where I is the real-time current value. Therefore, normalized real-time current change can be defined as $\Delta I/I_U = (I - I_U)/I_U$. To evaluate the precision of E-skin toward bending, the profile of ΔI versus θ were investigated at an applied voltage of 0.1 V, as shown in Figure 2d. With programed bending steps, the current of E-skin shows high consistency with bending angles (Figure 2d). In general, the relation between $\Delta I/I_U$ and θ can reflect the linearity and the sensitivity of flexion-sensitive E-skins. The device sensitivity represented by $\Delta I/I_U$ can eliminate the possible discrepancy of current value I_U in different devices. The

experimental data profile of $\Delta I/I_U$ versus θ (blue circles in Figure 2e) can be well fitted to a linear correlation (red line in Figure 2e), indicating the good linearity and high precision of as-prepared E-skin with a quantitative sensitivity of ≈0.04 rad^{-1}.

To further study the repeatability of PMMA/AFWCNT composite E-skin, the stepper was programed to run three repeated bending–unbending cycles at each θ. It was found that the I_U and $\Delta I/I_U$ values of each cycle at the same θ were almost identical (Figure 2f). This result hints at the high consistency and repeatability of the E-skin toward bending, which were considered as the crucial parameters for practical applications, such as soft robotics.[13,32] The response time of E-skin also exhibits approximately linear dependence with θ (Figure 2g), indicating its intrinsically high correlation toward θ and Δd, and also verifying the fast response of PMMA/AFWCNT composite E-skin.

The long-term durability of this E-skin was further certified by the fact that there was no performance degradation upon a prolonged process of 15 000 bending–unbending cycles (top image in Figure 2h). The device current I_U has very minor drift (less than 4%) induced by the slight change of "tube-to-tube" interface resistance during the very long-term cycling process. However, the normalized $\Delta I/I_U$ signals of bending–unbending cycles at the initial, middle, and ending stages of the long-term testing are very consistent and reproducible, as shown in the bottom of Figure 2h, indicating the good consistency and durability of AFWCNT composite based E-skins for continual use.

To understand the role of polymer matrix in composite E-skin, control devices of bare AFWCNT array paved on PET substrate without further spin-coating PMMA were prepared. As shown in **Figure 3**a, both Al/PMMA/AFWCNT/PET composite E-skin (black curve) and Al/AFWCNT/PET control device (red curve) demonstrate Ohmic conduction behavior. However, the conductivity of control device is about three times higher than the composite E-skin, owing to the lower interfacial resistance between AFWCNT array and Al electrodes. Typical bending–unbending cycles of these two devices are shown in Figure 3b. The difference of normalized current change $\Delta I/I_U$ between bending and unbending states of Al/PMMA/AFWCNT/PET composite E-skin (black curve) is about ten times higher than that of Al/AFWCNT/PET control device (red curve), demonstrating the much higher sensitivity and precision of composite E-skin toward bending. This result indicates that the device performance of flexion-sensitive E-skin is greatly enhanced by the introduction of PMMA coating. First, the interfacial resistance between AFWCNTs and metal electrodes is increased by PMMA wrapping (Figure 3a). Moreover, the PMMA filled in the gaps between the AFWCNTs can increase the lateral "tube-to-tube" resistance variation between nanotube bundles upon bending and unbending (Figure 3b). Thus, the response of PMMA/AFWCNT composite E-skin to bending is much stronger than that of Al/AFWCNT/PET control device.

For further comparison, control devices based on randomly dispersed few-walled CNT (RCNT) films prepared by vacuum

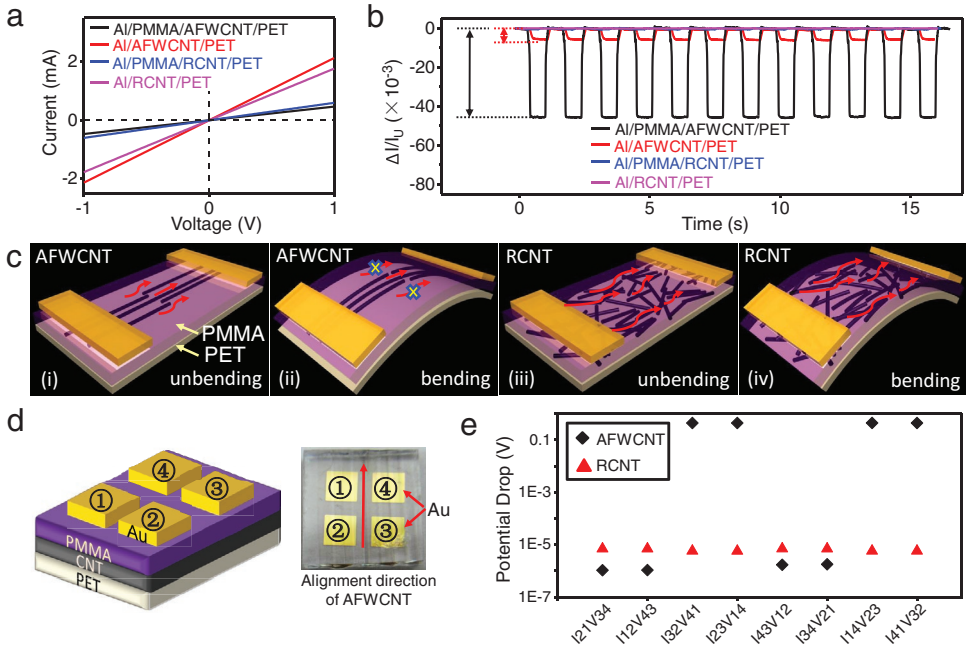

Figure 3. Performance and functioning mechanism comparisons of PMMA/AFWCNT based flexion-sensitive E-skin and control devices. a) Current value of Al/PMMA/AFWCNT/PET composite E-skin (black line) and control devices (Al/AFWCNT/PET, red line; Al/PMMA/RCNT/PET, blue line; Al/RCNT/PET, purple line) as a function of applied voltage at unbending state. b) Typical bending–unbending cycles at 70° of Al/PMMA/AFWCNT/PET E-skin and control devices at an applied voltage of 0.1 V. c) The differences of conductive behaviors and proposed functioning mechanisms between Al/PMMA/AFWCNT/PET E-skin (i and ii) and Al/PMMA/RCNT/PET control device (iii and iv). d) Schematic illustration (left image) and top view (right image) of the device setup for the electrical characterization of PMMA/CNT composite samples by van der Pauw method. e) The potential drops of one specific neighboring electrode pair on Al/PMMA/AFWCNT/PET E-skin (black dots) or Al/PMMA/RCNT/PET control device (red dots) with an applied current input of 10 μA on the other neighboring electrode pair. Typical *x* scale of I21V34 represents: constant current (10 μA) was input from electrode ② to electrode ① and the potential drop between electrodes ③ and ④ was monitored.

filtration (see the Experimental Section) were tested. Typical *I*–*V* curves at unbending state and bending–unbending cycles of Al/PMMA/RCNT/PET (blue curves) and Al/RCNT/PET control devices (purple curves) were shown in Figure 3a,b, respectively. The change of $\Delta I/I_U$ value during bending–unbending cycles of both Al/PMMA/RCNT/PET and Al/RCNT/PET control devices is very small (Figure 3b), indicating that the RCNT based control devices have almost no response to flexion, which is distinct from AFWCNT based devices. The possible functional mechanisms of Al/PMMA/AFWCNT/PET composite E-skin and Al/PMMA/RCNT/PET control device during bending–unbending cycles were compared in Figure 3c, showing that the distinct sensitivity toward bending is determined by the different current transport properties. For PMMA/AFWCNT-based E-skin, the device current at unbending state passes through AFWCNT bundles via hopping from bundles to bundles along the alignment orientation (Figure 3c-i). The flexion of bending state can cause the displacement and separation of closely connected AFWCNT bundles, which leads to the significant change of device resistance (Figure 3c-iii). However, for PMMA/RCNT-based control device, randomly connected CNTs formed a large amount of conductive connections (Figure 3c-iii). The interconnected RCNT network can conduct electricity in all directions, even in bending state (Figure 3c-iv). This isotropic conductive property makes the control devices based on PMMA/RCNT or RCNT film insensitive toward bending (blue and purple curves in Figure 3b). In contrast, the E-skin based on PMMA/AFWCNT composite shows high sensitivity owing to the anisotropic conductivity along the alignment direction and the distinct variation of interfacial resistance upon bending and unbending.

To prove the above assumptions about the current transport behaviors of PMMA/AFWCNT and PMMA/RCNT composite films, their electrical properties were further characterized by the van der Pauw method. The schematic illustration and top view of the device setup for van der Pauw measurements is shown in Figure 3d and the fabrication process is detailed in Experimental Section. Figure 3e shows the measured output voltages of one specific neighboring electrode pair of PMMA/AFWCNT (black dots) or PMMA/RCNT (red dots) composite films with an input current of 10 μA on the other electrode pair. For the PMMA/AFWCNT composite, when the current input and potential drop were along the alignment orientation of AFWCNT array (I12V34, I12V43, I43V12, and I34V21), the monitored potential drop was merely ≈1 μV. However, when the current input and potential drop of PMMA/AFWCNT composite film were in the perpendicular direction of AFWCNT alignment (I23V14, I32V41, I14V23, and I41V32), the monitored potential drop was about 0.8 V. The highly different potential drops of these two directions confirmed the anisotropic conductivity of PMMA/AFWCNT composite film. The ratio of electrical resistance along the alignment orientation and the perpendicular direction of AFWCNT array is about 10^5, indicating that the current prefers to transfer along the AFWCNT array rather than perpendicular to the direction of AFWCNT alignment. The large variation of "tube-to-tube" interfacial resistance between AFWCNT bundles upon bending (Figure 3c-ii) is the reason why PMMA/AFWCNT-based E-skin is very sensitive toward the flexion along the alignment direction of AFWCNT array. On the other hand, the potential drops of PMMA/RCNT composite film in the two directions exhibited a nearly identical value of ≈8 μV. This result indicates the isotropic conductivity of RCNT film, and the small change of electrical resistance during bending/unbending cycles can explain why the PMMA/RCNT-based control device is insensitive toward bending. To directly identify the structural change of PMMA/AFWCNT composite induced by bending, SEM and cathodoluminescence characterizations have been performed, as shown in Figure S1 (Supporting Information). The gaps between the AFWCNT bundles have been narrowed at bending state, indicating that the "tube-to-tube" interface and the interfacial resistance of AFWCNT array have been changed by bending.

Based on the above measurements and the understanding of the functioning mechanism, we further exhibit the practical application of E-skins. Considering the advantages of fast response and high precision toward bending angles, the flexion-sensitive E-skins were used to monitor the movement of human joints, such as fingers (**Figure 4**a).[32–34] The PMMA/AFWCNT-composite-based E-skins were covered/protected by an additional layer of Kepton polyimide tape, and then fixed at finger joints for the detection of bending–unbending motions

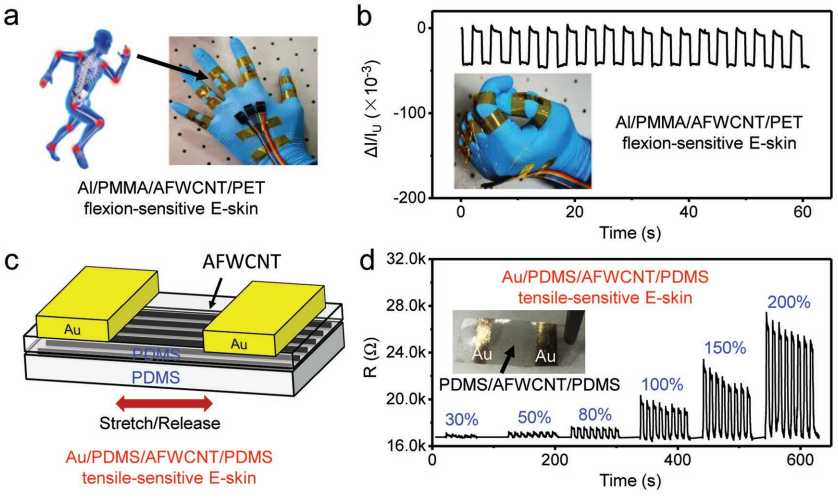

Figure 4. Tests of flexion-sensitive E-skins based on PMMA/AFWCNT composite and tensile-sensitive E-skins based on PDMS/AFWCNT composite. a) Schematic illustration (left) showing the application of flexion-sensitive E-skins for the detection of limb joint movements, and an optical image (right) of PMMA/AFWCNT E-skins attached on fingers with the assistance of Kepton polyimide tape. b) Current variation of flexion-sensitive E-skin during the finger bending–unbending cycles at an applied voltage of 0.1 V. The insert shows an optical image of flexion-sensitive E-skins fixed on fingers in bending state. c) Schematic illustration and d) performance of tensile-sensitive E-skin based on PDMS/AFWCNT composite. The resistance of tensile-sensitive E-skin was measured during stretching–releasing cycles at different strains with a constant applied voltage of 0.1 V. The insert shows an optical image of as-prepared tensile-sensitive E-skin.

(Figure 4a and the inset of Figure 4b). The current of E-skin increased rapidly upon bending the finger and fully recovered upon unbending (Figure 4b). This E-skin can be operated at 0.1 V with a device current at the magnitude of $\approx 10^{-4}$ A, indicating a very low power consumption (≈10 μW) that can be beneficial for future applications.

To demonstrate the versatility of polymer/AFWCNT composite for the detection of other movements, such as stretching,[35,36] a tensile-sensitive E-skin based on polydimethylsiloxane (PDMS)/AFWCNT composite was also built with a device structure different from the flexion-sensitive E-skin. Figure 4c shows the schematic of tensile-sensitive E-skin fabricated on PDMS substrate, which can detect the stretching and releasing along the aligned direction of AFWCNTs. Thermally evaporated gold (Au) electrodes were used in this E-skin because the adhesion of Au electrodes with PDMS is much better than that of Al electrodes. An optical image of as-prepared Au/PDMS/AFWCNT/PDMS E-skin is shown in the inset of Figure 4d, and the resistance change during stretching–releasing cycles at different extension ratios is shown in the main panel of Figure 4d. The device resistance increased instantly under stretching and then recovered to its original level upon releasing. As the extension ratio increased to higher levels (from 30% to 200%), the amplitude of resistance variation also increased accordingly. This result is ascribed to the large interfacial resistance change of the AFWCNT array at different extension ratios. This unique property will facilitate this E-skin to detect large strain with high sensitivity.

3. Conclusions

In summary, piezoresistive E-skins based on polymer/AFWCNT composite enabled by aligned carbon nanotubes exhibited multiple advantages, such as simple device structure, high precision, fast response, excellent stability, and low power consumption. It is expected that these novel devices with anisotropic sensing capabilities could be a promising candidate for applications in future bionic robots and wearable smart detectors.

4. Experimental Section

Materials and Chemicals: AFWCNT forests with a height of ≈4 mm and tube diameter of 3–5 nm were purchased from Suzhou Jiedi Nano Technology Co., Ltd. PMMA (analytical standard, molecular weight 4000) was purchased from Sigma-Aldrich. RCNT powder with similar tube diameter (3–5 nm) and a length distribution of 5–30 μm was purchased from Chengdu Organic Chemical Co., Ltd. Mixed cellulose ester membranes with 200 nm pores were purchased from J&K Chemicals. PDMS Sylgard-184 was purchased from Dow Corning Corp. Other materials and chemicals, such as PET, anisole, and alcohol, were purchased from Alfa Aesar.

Fabrication of PMMA/AFWCNT Based Flexion-Sensitive E-Skin: First, pave the AFWCNT array pulled out from the AFWCNT forest by tweezers (top image in Figure 1b) onto a PET film (0.8 mm thick), then treat it with alcohol vapor at 70 °C to tightly adhere AFWCNT array to the PET substrate. Second, spin-coat the anisole solution of 90 mg mL^{-1} PMMA onto AFWCNT array with a rotation speed of 3000 rpm for 1 min, and then anneal the substrate at 90 °C for 10 min. Finally, deposit a pair of Al or Au electrodes with 100 nm thickness onto the surface of PMMA/AFWCNT composite via shadow-masked thermal evaporation. In this way, flexion-sensitive E-skin based on PMMA/AFWCNT composite was fabricated. The control device of Al/AFWCNT/PET was fabricated with a similar process but without the spin-coating and annealing of PMMA. For the detection of finger bending motions, flexion-sensitive E-skin (0.5 cm × 2.0 cm) and welded electric wires were fixed on the finger joints by the assistance of Kepton polyimide tape.

Fabrication of RCNT Based Control Devices: 3.0 mg of RCNT powder was dispersed into 200 mL of 1.0 wt% sodium dodecyl benzene sulfonate aqueous solution under ultrasonication. Then, the suspension was vacuum-filtrated with a mixed cellulose ester membrane to obtain RCNT film. The mixed cellulose ester membrane was dissolved with acetone and the freestanding RCNT film was transferred onto the PET substrate for the fabrication of Al/PMMA/RCNT/PET and Al/RCNT/PET control devices. The fabrication processes of RCNT based control devices are similar to those of AFWCNT based devices.

Fabrication of PDMS/AFWCNT Based Tensile-Sensitive E-Skins: First, AFWCNT array was paved onto the PDMS substrate (normally 3.0 cm length × 1.0 cm width × 0.15 cm height). Second, *n*-hexane diluted PDMS precursor (500 mg mL^{-1}) was spin-coated onto AFWCNT/PDMS with a rotation speed 3000 rpm for 1 min and then, the spin-coated PDMS film was solidified at 90 °C for 30 min. Finally, a pair of Al or Au electrodes with 100 nm thickness was deposited onto the substrate by shadow-masked thermal evaporation.

Characterizations: SEM was performed on Hitachi S-4800 with an operation voltage of 1.0 kV and a working distance of 8.2 mm. Topographic AFM and conductive AFM were performed on Bruker Dimension Icon with tapping mode. Conductive AFM was performed under a bias voltage of 3.0 V with a Pt-coated PFTUNA probe.

Performance Measurements of Devices: Flexion-sensitive E-skins were bent and unbent with a programmable motor-controlled stepper (Beijing Optical Century Instrument Corp). The designated device was fixed on the stepper by two clippers and the stepper was set to work in a pulse mode with a frequency of 2.0 kHz and a step size of 25 μm. The current–voltage and current–time curves of the as-prepared devices were collected with a Keithley 2635 source meter.

For van der Pauw tests, four square Au electrodes were evaporated onto PMMA/AFWCNT/PET or PMMA/RCNT/PET device with the assistance of shadow mask. Then, the device was characterized with one neighboring electrode pair as current input (10 mA) and the other neighboring electrode pair as voltage output.

For the tests of PDMS/AFWCNT-based tensile-sensitive E-skin, the device was stretched and released by fixing one electrode with a clipper on an optical bread plate and clipping the other electrode on the stepper. The stepper moves back and forth in a pulse mode with a frequency of 2.0 kHz and a step size of 25 μm. The electrical properties of the tensile-sensitive E-skin were also characterized with Keithley 2635 source meter.

Supporting Information

Supporting Information is available from the Wiley Online Library or from the author.

Acknowledgements

This work was supported by the National Natural Science Foundation of China (Grant Nos. 21403105 and 21573108), National 973 Basic Research Program (Grant No. 2015CB659300), National Materials Genome Project (Grant No. 2016YFB0700600), China Postdoctoral Science Foundation (Grant Nos. 2015M581775 and 2015M580413), Natural Science Foundation for Young Scholars of Jiangsu Province (Grant Nos. BK20150583 and BK20160647), Fundamental Research Funds for the Central Universities and a project funded by the Priority Academic Program Development (PAPD) of Jiangsu Higher Education Institutions.

Keywords

aligned few-walled carbon nanotube arrays, electronic skins, flexion-sensitive, polymer composites, tensile-sensitive

Received: December 14, 2016
Revised: February 14, 2017
Published online: March 30, 2017

[1] S. C. B. Mannsfeld, B. C. K. Tee, R. M. Stoltenberg, C. V. H. H. Chen, S. Barman, B. V. O. Muir, A. N. Sokolov, C. Reese, Z. Bao, *Nat. Mater.* **2010**, *10*, 859.
[2] F. Zhang, Y. Zang, D. Huang, C. A. Di, D. Zhu, *Nat. Commun.* **2015**, *6*, 8356.
[3] M. Segev-Bar, H. Haick, *ACS Nano* **2013**, *10*, 8366.
[4] H.-H. Chou, A. Nguyen, A. Chortos, J. W. F. To, C. Lu, J. Mei, T. Kurosawa, W.-G. Bae, J. B. H. Tok, Z. Bao, *Nat. Commun.* **2015**, *6*, 8011.
[5] X. L. Zhao, Q. L. Hua, R. M. Yu, Y. Zhang, C. F. Pan, *Adv. Electron. Mater.* **2015**, *1*, 1500142.
[6] M. L. Hammock, A. Chortos, B. C. K. Tee, J. B. H. Tok, Z. Bao, *Adv. Mater.* **2013**, *42*, 5997.
[7] T. Someya, T. Sekitani, S. Iba, Y. Kato, H. Kawaguchi, T. P. Sakurai, *Proc. Natl. Acad. Sci. USA* **2004**, *27*, 9966.
[8] W. Honda, S. Harada, T. Arie, S. Akita, K. Takei, *Adv. Funct. Mater.* **2014**, *22*, 3299.
[9] X. Wang, Y. Gu, Z. Xiong, Z. Cui, T. Zhang, *Adv. Mater.* **2014**, *9*, 1336.
[10] D. Son, J. Lee, S. Qiao, R. Ghaffari, J. Kim, J. E. Lee, C. Song, S. J. Kim, D. J. Lee, S. W. Jun, S. Yang, M. Park, J. Shin, K. Do, M. Lee, K. Kang, C. S. Hwang, N. Lu, T. Hyeon, D.-H. Kim, *Nat. Nanotechnol.* **2014**, *9*, 397.
[11] K. Takei, T. Takahashi, J. C. Ho, H. Ko, A. G. Gillies, P. W. Leu, R. S. Fearing, A. Javey, *Nat. Mater.* **2010**, *10*, 821.
[12] C. Wang, D. Hwang, Z. Yu, K. Takei, J. Park, T. Chen, B. Ma, A. Javey, *Nat. Mater.* **2013**, *10*, 899.
[13] G. Canavese, S. Stassi, C. Fallauto, S. Corbellini, V. Cauda, V. Camarchia, M. Pirola, C. F. Pirri, *Sens. Actuators A* **2014**, *208*, 1.
[14] J. Park, Y. Lee, J. Hong, M. Ha, Y.-D. Jung, H. Lim, S. Y. Kim, H. Ko, *ACS Nano* **2014**, *5*, 4689.
[15] S. Yao, Y. Zhu, *Nanoscale* **2014**, *4*, 2345.
[16] D. J. Lipomi, M. Vosgueritchian, B. C.-K. Tee, S. L. Hellstrom, J. A. Lee, C. H. Fox, Z. Bao, *Nat. Nanotechnol.* **2011**, *12*, 788.
[17] Z. F. Liu, S. Fang, F. A. Moura, J. N. Ding, N. Jiang, J. Di, M. Zhang, X. Lepró, D. S. Galvão, C. S. Haines, N. Y. Yuan, S. G. Yin, D. W. Lee, R. Wang, H. Y. Wang, W. Lv, C. Dong, R. C. Zhang, M. J. Chen, Q. Yin, Y. T. Chong, R. Zhang, X. Wang, M. D. Lima, R. Ovalle-Robles, D. Qian, H. Lu, R. H. Baughman, *Science* **2015**, *6246*, 400.
[18] C. Dagdeviren, Y. Su, P. Joe, R. Yona, Y. Liu, Y.-S. Kim, Y. Huang, A. R. Damadoran, J. Xia, L. W. Martin, Y. Huang, J. A. Rogers, *Nat. Commun.* **2014**, *5*, 4496.
[19] W. Wu, X. Wen, Z. L. Wang, *Science* **2013**, *6135*, 952.
[20] F.-R. Fan, L. Lin, G. Zhu, W. Wu, R. Zhang, Z. L. Wang, *Nano Lett.* **2012**, *6*, 3109.
[21] C.-L. Choong, M.-B. Shim, B.-S. Lee, S. Jeon, D.-S. Ko, T.-H. Kang, J. Bae, S. H. Lee, K.-E. Byun, J. Im, Y. J. Jeong, C. E. Park, J.-J. Park, U. I. Chung, *Adv. Mater.* **2014**, *21*, 3451.
[22] C. Pan, L. Dong, G. Zhu, S. Niu, R. Yu, Q. Yang, Y. Liu, Z. L. Wang, *Nat. Photonics* **2013**, *9*, 752.
[23] K.-Y. Chun, Y. Oh, J. Rho, J.-H. Ahn, Y.-J. Kim, H. R. Choi, S. Baik, *Nat. Nanotechnol.* **2010**, *12*, 853.
[24] T. Yamada, Y. Hayamizu, Y. Yamamoto, Y. Yomogida, A. Izadi-Najafabadi, D. N. Futaba, K. Hata, *Nat. Nanotechnol.* **2011**, *5*, 296.
[25] J. Zoldan, A. Siegmann, M. Narkis, *Polym. Eng. Sci.* **2006**, *9*, 1250.
[26] B. C. Tee, C. Wang, R. Allen, Z. Bao, *Nat. Nanotechnol.* **2012**, *12*, 825.
[27] Q. Wang, X. Qian, S. Wang, W. Zhou, H. Guo, X. Wu, J. Li, X. Wang, *Synth. Met.* **2015**, *199*, 1.
[28] T. Takahashi, K. Takei, A. G. Gillies, R. S. Fearing, A. Javey, *Nano Lett.* **2011**, *12*, 5408.
[29] X. Xiao, L. Yuan, J. Zhong, T. Ding, Y. Liu, Z. Cai, Y. Rong, H. Han, J. Zhou, Z. L. Wang, *Adv. Mater.* **2011**, *45*, 5440.
[30] F. Meng, X. Zhang, G. Xu, Z. Yong, H. Chen, M. Chen, Q. Li, Y. Zhu, *ACS Appl. Mater. Interfaces* **2011**, *3*, 658.
[31] J. Di, D. Hu, H. Chen, Z. Yong, M. Chen, Z. Feng, Y. Zhu, Q. Li, *ACS Nano* **2012**, *6*, 5457.
[32] R. C. Webb, A. P. Bonifas, A. Behnaz, Y. Zhang, K. J. Yu, H. Cheng, M. Shi, Z. Bian, Z. Liu, Y.-S. Kim, W.-H. Yeo, J. S. Park, J. Song, Y. Li, Y. Huang, A. M. Gorbach, J. A. Rogers, *Nat. Mater.* **2013**, *10*, 938.
[33] C. Yan, J. Wang, W. Kang, M. Cui, X. Wang, C. Y. Foo, K. J. Chee, P. S. Lee, *Adv. Mater.* **2014**, *13*, 2022.
[34] S. Chen, Z. Lou, D. Chen, K. Jiang, G. Shen, *Adv. Mater. Technol.* **2016**, *7*, 1600136.
[35] M. Amjadi, A. Pichitpajongkit, S. Lee, S. Ryu, I. Park, *ACS Nano* **2014**, *5*, 5154.
[36] S. Ryu, P. Lee, J. B. Chou, R. Xu, R. Zhao, A. J. Hart, S.-G. Kim, *ACS Nano* **2015**, *6*, 5929.

